Ion Beam Divergence Characteristics of Two-Grid Accelerator Systems

G. Aston,* H. R. Kaufman,† and P. J. Wilbur‡
Colorado State University, Fort Collins, Colo.

The first comprehensive experimental investigation of two-grid accelerator systems is presented. A wide range of geometrical grid parameters and grid set operating conditions were investigated for their effect on ion beam divergence. Ion beam divergence was found to depend most strongly on normalized perveance per hole, grid separation ratio, net-to-total accelerating voltage ratio, and discharge-to-total accelerating voltage ratio variations. The graphical results contained herein provide guidelines for the design of ion accelerator systems. A general ion beam divergence angle correlation was developed to permit approximate beam divergence estimates, at parameteric values other than those tested, of present grid set designs. Although argon was the main test gas used in this study, it is shown that the results are applicable to other propellants as well.

Nomenclature

ℓ_g = grid separation distance
d_s = screen hole diameter
d_a = accelerator hole diameter
d_b = beamlet diameter
t_s = screen grid thickness
t_a = accelerator grid thickness
ℓ_e = effective acceleration length
V_T = total accelerating voltage
V_n = net accelerating voltage
V_D = discharge voltage
V_S = sheath potential
V_p = plasma potential
R = net-to-total accelerating voltage ratio
α = ion beam divergence angle
f_D = ion beam divergence factor
J_B = beam current per hole
q = ion charge
ϵ_0 = free space permittivity
M_i = ion mass
Φ_i = propellant first ionization potential

I. Introduction

KNOWLEDGE of the ion§ beam divergence characteristics of multiaperture accelerator systems is important for both electric space propulsion and ground applications of electron-bombardment ion sources. A highly collimated beam (minimum off-axis ion velocity components) is generally preferred for both space and ground applications. The amount of ion beam divergence depends on the geometrical grid parameters and operating conditions of the accelerator system. Theoretical approaches used to date for predicting the performance of multiaperture accelerator systems have shown general trends only.[1-4] These theoretical approaches have dealt with single aperture accelerator systems. Previous experimental results have shown differences in the ion beam divergence characteristics of single and multiaperture accelerator systems.[5] A detailed experimental investigation was therefore undertaken to determine ion beam divergence over a wide range of geometrical parameters and operating conditions for multiaperture accelerator systems. SI (rationalized mks) units are used throughout this paper.

Received Sept. 9, 1977; revision received Jan. 17, 1978.

Index category: Electric and Advanced Space Propulsion.

*Research Assistant, Departments of Physics. Student Member AIAA.

†Professor, Departments of Physics and Mechanical Engineering. Associate Fellow AIAA.

‡Associate Professor, Department of Mechanical Engineering. Member AIAA.

§Since this work deals only with singly charged positive ions, the term "ion" is used with the exclusive meaning "singly charged positive ion."

II. Ion Beam Formation

The ion extraction system chosen for this study was the two-grid accelerator geometry common to most electron-bombardment ion sources. Figure 1a depicts a portion of this multiaperture system showing the coaxial hole geometry and ion beamlet formation. Figure 2 illustrates the variation in electrical potential associated with the grid geometry of Fig. 1a.

A low-density singly ionized plasma is generated within a discharge chamber by electron-bombardment of neutral propellant atoms. The discharge chamber is at a potential a few tens of volts positive of the screen grid, which is at a high positive potential (Fig. 2). Around each screen hole a stable plasma sheath is formed. This sheath is a space charge limited emissive surface of positive ions from the discharge plasma. The ions reach the sheath with the Bohm velocity[6] and are accelerated by the strong electric field between the positive sheath and negative accelerator grid hole (Fig. 2). Depending

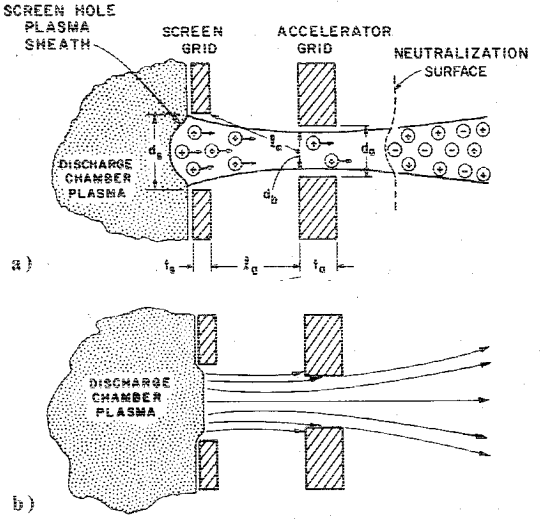

Fig. 1 Ion beamlet formation, a) normal accelerator system operation, b) high impingement operation.

upon the amount of focusing that occurs, most of the ions will pass through the accelerator grid hole and be ejected at high velocity into the downstream side of the grid.

The ion, or beam current, leaving the accelerator system is space charge limited, so that the accelerator system resembles a vacuum diode. The perveance for a parallel plate diode can be obtained from Child's law[7]

$$\frac{J_B}{V_T^{3/2}} = \frac{\pi\epsilon_0}{9}\left(\frac{2q}{M_i}\right)^{1/2}\left(\frac{d_s}{\ell}\right)^2 \tag{1}$$

Here the length ℓ refers to the plate separation. The assumption has been made that the area of ion emission is $\pi d_s^2/4$. This planar expression has been found to agree fairly well with the maximum beam current capacity per hole for a two-grid accelerator system if the effective acceleration length ℓ_e[4] is used in place of ℓ, where

$$\ell_e = [\ell_g^2 + (d_s^2/4)]^{1/2} \tag{2}$$

With this substitution, beam current variations may be expressed in terms of normalized perveance per hole

$$\frac{J_B}{V_T^{3/2}}\left(\frac{\ell_e}{d_s}\right)^2 = \frac{\pi\epsilon_0}{9}\left(\frac{2q}{M_i}\right)^{1/2} \tag{3}$$

Equation (3) indicates that there is an upper limit to the normalized perveance per hole for a particular propellant. For mercury, the propellant of interest for electric space propulsion, this maximum value is 3.03×10^{-9} A/V$^{3/2}$. For argon, the test gas used in this study, this maximum value is 6.79×10^{-9} A/V$^{3/2}$. Normalized perveance per hole, $(J_B/V_T^{3/2})\,(\ell_e/d_s)^2$, will be used to describe the ion extraction performance of each grid set investigated.¶

Ion focusing effects occur in two regions of the accelerator system: between the grids and just downstream of the grids. Ions between the grids tend to follow the electric field lines passing from the screen hole plasma sheath through the accelerator hole. This tendency to follow electric field lines is most evident near the plasma sheath, where the ion velocity is small. The position and shape of the screen hole plasma sheath is crucial to this phase of the ion focusing process because it determines the local accelerating electric field distribution. Both screen hole plasma sheath position and shape depend on the ion current being extracted and the accelerator system geometry. In normal operation, the shape of the plasma sheath is similar to that shown in Fig. 1a. As plasma density increases, the sheath moves further into the screen hole to satisfy the requirement of space charge limited ion current emission from the discharge chamber plasma. The sheath shape becomes flatter and direct ion impingement upon the accelerator grid begins to occur (Fig. 1b). Further plasma density increases only result in further ion focusing degradation. In practice, high impingement limits the ion current which can be extracted from an accelerator system.

As the focused ions leave the accelerator system, electrons are injected into the beam to maintain a neutral charge efflux. These neutralization electrons spread rapidly throughout the beam producing a neutral plasma. Because of the negative accelerator grid potential, neutralization electrons which approach the accelerator holes are repulsed by electrostatic forces. The result is a neutralization, or equipotential, surface created slightly downstream from the accelerator grid which is

¶It has been suggested by a reviewer that the fraction F, of the maximum possible Child's law current, be used to describe the ion extraction performance of each grid set. For argon, F would be defined as $F \equiv (6.79\times10^{-9})^{-1}\,(J_B/V_T^{3/2})\,(\ell_e/d_s)^2$ and would be expected to range from 0 to 1. The approximations used in applying Child's law to this system can result in values of F somewhat greater than 1.0,[10] but use of F would permit all propellants to be put on one scale.

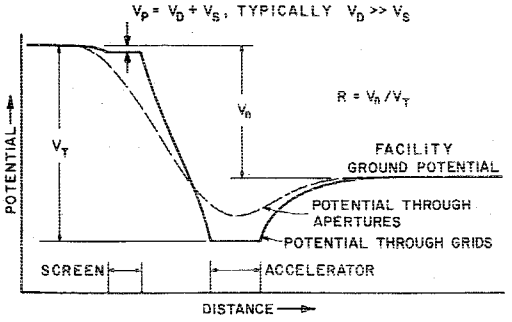

Fig. 2 Accelerator system potential variation.

at approximately facility ground potential (Fig. 1a). Between the accelerator holes and the neutralization surface the ions are decelerating through a region of retarding electric field (Fig. 2). Although the deceleration incurred is less than the acceleration imparted by the grid set, it is still sufficient to defocus the ion trajectories significantly. However, once these ions reach the neutralization surface, electrostatic shielding by the beam plasma nullifies the accelerator grid effect, and little additional change in ion trajectories occurs. The amount of ion defocusing in this downstream region depends on the net-to-total accelerating voltage ratio R (Fig. 2). Ion defocusing decreases as R increases, so it would appear desirable to have R as near unity as possible. In practice, however, a value of $R = 1.0$ cannot be reached because neutralization electrons will backstream to the discharge chamber plasma when the negative accelerator grid potential is sufficiently small.

Both regions of ion focusing mentioned earlier were examined for their contribution to the overall ion beam divergence. Ion focusing between the grids was varied by changing the beam current (i.e., the ion current leaving the accelerator system), the accelerator system geometry, and the total accelerating and discharge voltages. Ion defocusing was varied by changing the net-to-total accelerating voltage ratio.

III. Apparatus and Procedure

For this study, a mildly divergent magnetic field 8-cm-diam electron-bombardment ion source was constructed. Tungsten wire filaments were used as both the main and neutralizer cathode emitters. The magnetic field was derived from a long solenoidal winding extending the length of the discharge chamber, with additional coil windings positioned at the chamber's upstream end. The coil geometry was such that the field strength at the downstream end of the discharge chamber was 60% that of the upstream end. A cylindrical anode was employed and nonmagnetic stainless steel construction used throughout the source. Further design details and operating characteristics for this type of source can be found in the literature.[8,9] Mercury is the propellant of principle interest for electric space propulsion, but because of the difficulty in changing ion source operating conditions rapidly with mercury it was not used for this study. Argon was chosen as propellant because of its availability and the ease and speed with which flow rates could be set and altered.

The screen and accelerator grids were made from thin flat sheet graphite. The grid aperture pattern used comprised a 19-hole hexagonal array with a center-to-center hole spacing of 2.54 mm. It was felt that this number of holes adequately modeled the adjacent screen hole interactions found in full-size grid systems. Variable grid separation was accomplished by using various numbers of thin mica washers (0.254-mm thick). The grid sets were fastened together with four insulated stainless steel bolts. Alignment of the screen and accelerator grids was done by hand beneath a large illuminated magnifying glass; this straightfoward technique was found to produce good data reproducibility. The assembled accelerator system (measuring 5-cm square) was placed on a masked down discharge chamber, which insured

ion extraction from a near uniform plasma. Calculations predicted the greatest spatial variation in discharge chamber plasma density across the 1-cm^2 hexagonal hole array would be less than 5%. Grid separation could be checked with feeler gages when cold, but while the source was operating and the grids were hot they could only be examined visually. While some grid warpage could occur during operation, the magnitude of this warpage should be small because the grids were made of carbon, and the greatest distance between grid supports was less than 2 cm. All source operation was conducted in a 30-cm pyrex bell jar. Average bell jar pressure was 1×10^{-4} Torr.

Beam divergence measurements were accomplished using a movable probe rake containing 20 individual Faraday ion current sensors. A more complete discussion of the Faraday probe rake design and construction is contained in a previous publication.[10] This probe rake was positioned normal to the beam axis and 16.7 cm downstream of the accelerator system. (The grid set-to-probe rake separation distance actually varied from 8.5 to 22.5 cm, with most of the data obtained at a separation of 16.7 cm. Grid set-to-probe rake separation variations did not seem to affect the beam divergence angle measurements.) Figure 3 shows the ion source and probe rake in position. The probes were screened and biased to reflect neutralization electrons and low-energy charge exchange ions present in the beam plasma. After stable source operation was obtained, the probe rake was centered along the beam axis. Beam current was varied by adjusting the refractory cathode current and hence electron emission and discharge chamber plasma density. Each grid set geometry investigated was operated over a range of increasing emission levels to the maximum beam current obtainable from that grid set. The approach to this maximum was usually characterized by a rapid increase in accelerator grid impingement current and a negligible beam current increase. Ion beam profiles were obtained at selected beam currents leading up to this maximum. Each profile consisted of 20 ion current density measurements, corresponding to the ion current received by each Faraday probe as a function of its position normal to the beam axis. Figure 3 shows a typical ion beam profile. From these profiles ion beam divergence could be measured quantitatively by calculating the ion beam divergence angle α (Fig. 3). The ion beam divergence angle was defined as the truncated cone angle enclosing 95% of the total integrated beam current. The total integrated beam current, after appropriate corrections, always agreed closely with the measured accelerator system beam current. Another less obvious parameter for determining ion beam divergence is the ion beam divergence factor f_D. This quantity is of considerable interest for ion thruster applications of electron-bombardment ion sources. The divergence factor is the ratio of the net axial thrust produced by the divergent ion beam to the thrust that would be produced if the ion beam were perfectly collimated. Both ion beam divergence angle and ion beam divergence factor were the calculated parameters (based on experimental measurements) of primary interest to this study. The following equations were used in their determination:

$$\alpha=\tan^{-1}[(R_\alpha-R_B)/L] \tag{4}$$

$$f_D=\sum_{i=1}^{77} J_iR_i\cos\theta_i\Big/\sum_{i=1}^{77} J_iR_i \tag{5}$$

where

R_α = radius normal to the beam axis defining a cone enclosing 95% of the total integrated beam current

R_B = ion beam radius at accelerator grid

L = grid set-to-probe rake separation distance

J_i = probe current for the ith probe (an interpolation routine was used to increase the number of probe data points from 20 to 77)

R_i = distance from ion beam axis to ith probe

θ_i = angle formed by intersection of a line extending from the edge of the grid set hole array to the ith probe and the ion beam axis.

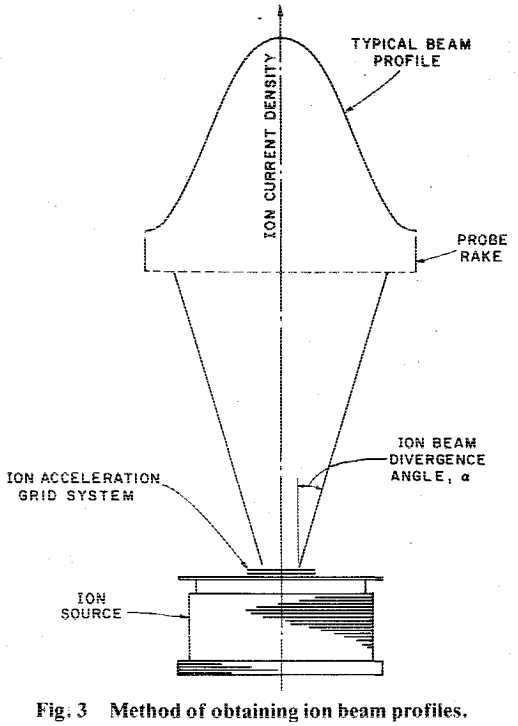

Fig. 3 Method of obtaining ion beam profiles.

IV. Results and Discussion

The effect of grid geometry variations on ion beam divergence was determined by independently varying the grid separation distance ℓ_g, accelerator hole diameter d_a, screen grid thickness t_s, and accelerator grid thickness t_a. To nondimensionalize the geometrical grid parameters they were divided by the screen hole diameter d_s, which remained at 2.06 mm throughout this study. The precision of the data obtained was verified by repeatedly testing various grid set geometries at different times with the grids reassembled and realigned for each test. The results of these tests showed a maximum variation in α and f_D of ±0.5 deg and ±0.001, respectively. The absolute accuracy of the data is thought to be better than $\pm$ 1 deg for α, and better than ±0.002 for f_D. A tabular listing of all the experimental results obtained during this study is contained in a previous publication.[11]

Figure 4 shows the effect of propellant flow rate variation on ion beam divergence for a particular grid geometry. This grid geometry, the total accelerating voltage, discharge voltage, and net-to-total accelerating voltage ratio are typical of values presently used in mercury ion thrusters[12,13] and ground-based argon ion sources.[14,15] An almost fivefold variation in flow rate is seen not to alter substantially the grid systems divergence characteristics. A small, consistent, beam divergence angle decrease with increasing propellant flow rate is, however, shown in Fig. 4. This trend has been reported previously by Alterburg et al.[16] The present data verify those observations. For very small flow rates the discharge became unstable and extinguished before any accelerator system limitation was reached (circles in Fig. 4). Large electron temperature increases, as the beam current was increased at low flow rates, may be responsible for the discharge extinguishing. It is sufficient, though, to note that the source would not operate when the propellant flow rate, or neutral atom discharge chamber pressure, was too low. In practice, the ion source was operated at the minimum flow rate which would give stable source operation up to the maximum beam

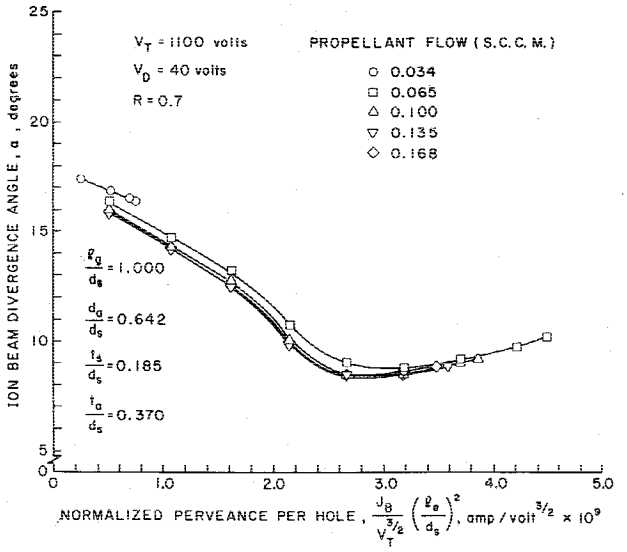

Fig. 4 Effect of propellant flow rate variations on ion beam divergence.

current obtainable from the grid set being tested. This resulted in a propellant flow rate which varied from 0.075 to 0.125 standard cubic centimeters per minute (S.C.C.M.) over the range of grid set geometries and operating conditions investigated. Figure 4 shows that these flow rate variations should produce a negligible effect on the ion beam divergence characteristics of a particular grid set geometry.

Figure 4 shows also that there is an optimum perveance corresponding to an optimum screen hole sheath position and shape which gives the lowest ion beam divergence angle. This minimum divergence angle defines the accelerator system operating condition most desirable from an ion focusing viewpoint. It is interesting to note that grid set operation at the minimum beam divergence angle is also close to the maximum beam current at which one would usually operate. Increasing the beam current further, and thereby allowing the screen hole sheath to become flatter in shape (Fig. 1b), results in an increasing fraction of accelerated ions impinging directly upon the accelerator grid. The associated increase in ion sputtering damage seriously degrades acceleratror grid lifetime.

Figures 5 and 6 show the beam divergence variation for changes to the grid separation ratio ℓ_g/d_s and net-to-total accelerating voltage ratio R. For these data, the accelerator hole diameter ratio d_a/d_s, screen grid thickness ratio t_s/d_s, and accelerator grid thickness ratio t_a/d_s were held constant at values of 0.642, 0.185, and 0.370, respectively. Qualitatively, all curve shapes are similar. This similarity in curve shape and the fact that variations in the maximum normalized perveance per hole** are small indicates the usefulness of normalized perveance per hole as a correlating parameter. Increasing the grid separation ratio for a constant net-to-total accelerating voltage ratio, decreases ion beam divergence angles, with corresponding ion beam divergence factor increases. This results from the more planar equipotential surfaces asssociated with a longer grid separation distance. Similarly, increasing the net-to-total accelerating voltage ratio for a constant grid separation ratio decreases overall ion beam divergence, as was mentioned previously in Sec. II. This effect was greatest for the smallest grid separation ratio tested and decreased with grid separation ratio increases. Also, the effect beam current variations have on ion beam divergence decreases with decreasing values of R.

**It is important to realize that constant normalized perveance per hole does not mean constant beam current. If the total accelerating voltage, V_T, is held constant, the beam current will increase as the grid separation ratio is decreased [Eq. (3)].

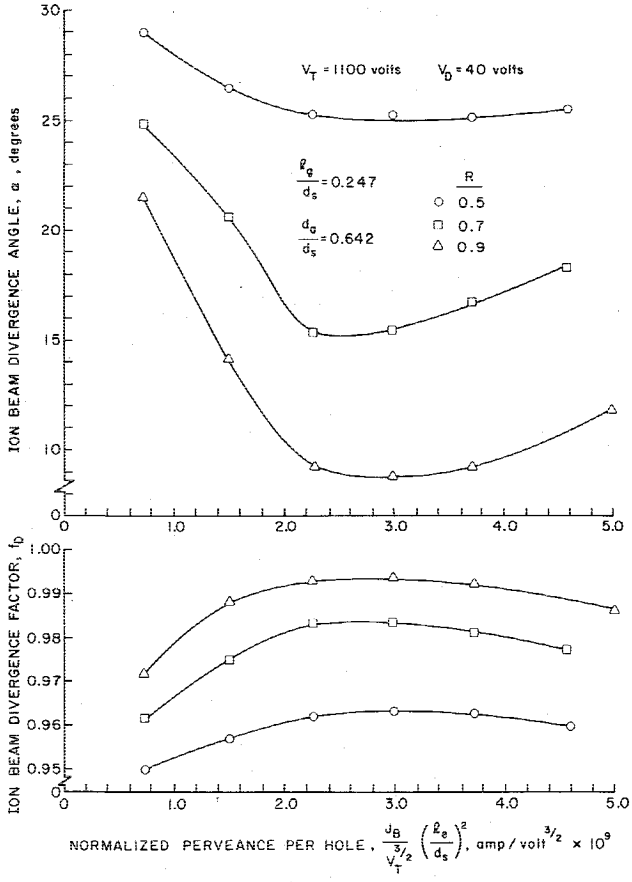

Fig. 5 Effect of R on ion beam divergence (small grid separation ratio, $\ell_g/d_s = 0.247$).

Figures 5 and 6 show that large ion beam divergence variations are possible with two-grid accelerator systems. A reduction in the minimum ion beam divergence angle from 25.1 deg to 4.9 deg is observed when going from values of $\ell_g/d_s = 0.247$ and $R = 0.5$ to $\ell_g/d_s = 1.000$ and $R = 0.9$.

Figure 7 shows the effect variations in the accelerator hole diameter ratio d_a/d_s have on ion beam divergence. Only slight beam divergence angle changes are observed for large variations in this parameter. However, decreasing the accelerator hole diameter ratio substantially decreases the maximum normalized perveance per hole, or beam current, obtainable from the grid set. A larger accelerator hole allows the screen hole plasma sheath to penetrate further into the screen hole, with reduced ion focusing (Fig. 1b), before an excessive accelerator grid ion impingement current is reached. Larger accelerator holes result therefore in increased beam currents. Of particular interest in Fig. 7 are the results obtained with the smallest accelerator hole diameter ratio tested. Here, the beam divergence angle actually goes through a maximum with increasing beam current. The accelerator grid impingement current observed with this grid set was large at the smallest beam current, went through a minimum as beam current was increased, and then rose sharply as the maximum beam current was approached. These characteristics suggest ion trajectory crossover may be occurring at low beam current levels.[17] If this is occurring, the apparent decrease in divergence angle at very low perveances could be caused by ions that leave the screen hole sheath edge and impinge directly upon the accelerator grid. Hence, the accelerator grid is acting as a beamlet mask for severe off-axis velocity ions at very small accelerator hole diameter ratios.

Figure 8 shows the effect variations in the accelerator grid thickness ratio t_a/d_s have on ion beam divergence. Only slight beam divergence angle changes are observed for large variations in this parameter. These beam divergence angle

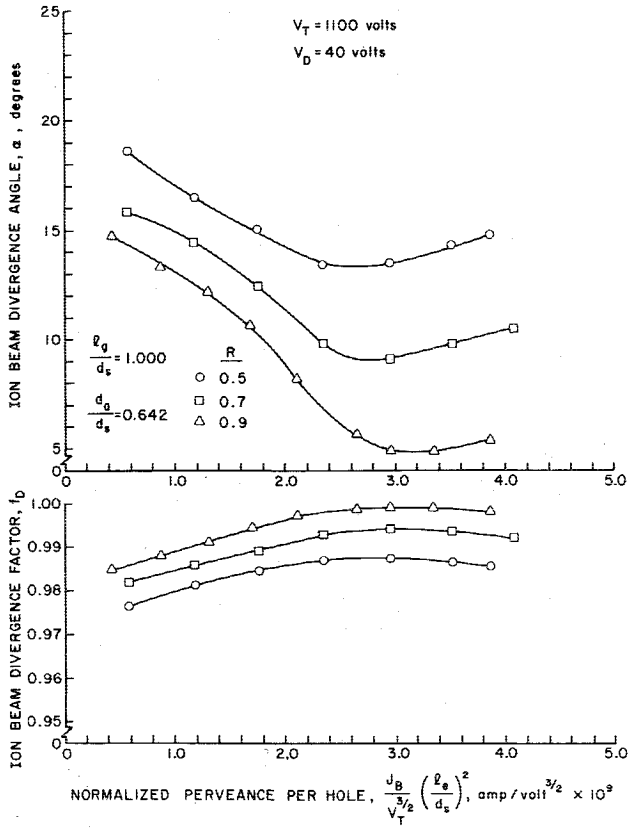

Fig. 6 Effect of R on ion beam divergence (very large grid separation ratio, $\ell_g/d_s = 1.000$).

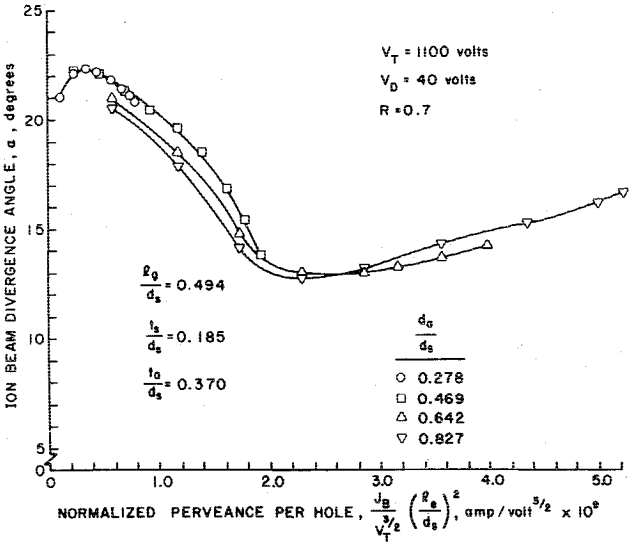

Fig. 7 Effect of accelerator hole diameter ratio d_a/d_s on ion beam divergence.

changes increase with increasing normalized perveance, or beam current. A thicker accelerator grid means a longer distance for each beamlet ion to travel in a region where little, if any, axial acceleration is being imparted to it. While the central region of a thick accelerator grid hole is fairly uniform in potential, the edge regions are not and produce electric fields directed towards the accelerator hole edge. The larger the accelerator grid thickness ratio, the longer each beamlet ion is subjected to these edge, or fringe, fields. At low normalized perveance-per-hole values, the beamlet diameter passing through the accelerator hole is small, so that the beamlet ions are in a region of near uniform potential and

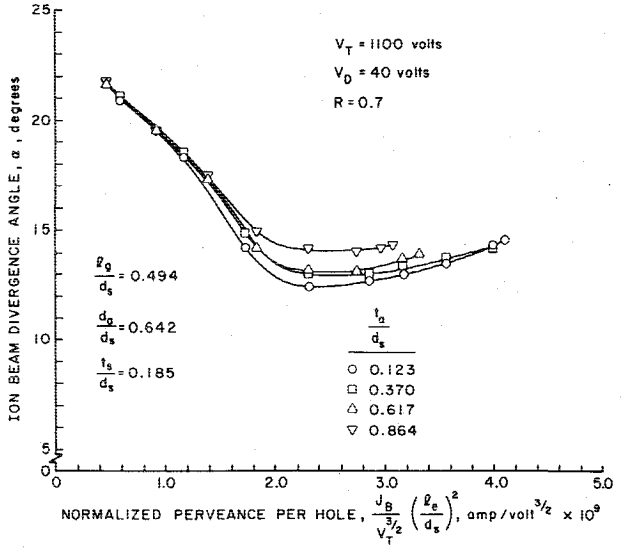

Fig. 8 Effect of accelerator grid thickness ratio t_a/d_s on ion beam divergence.

accelerator grid thickness ratio variations would not be expected to affect ion beam divergence. However, at high normalized perveance-per-hole values the beamlet diameter is approaching that of the accelerator hole and those ions along the beamlet edge would be deflected more towards the accelerator hole edge with increasing accelerator grid thickness ratio. This effect would lead to larger ion beam divergence angles and increased accelerator grid impingement currents, causing decreased maximum normalized perveance-per-hole values as the accelerator grid thickness ratio is increased (Fig. 8). Variations in the screen grid thickness ratio t_s/d_s were investigated also for their effect on ion beam divergence. Changes to the minimum ion beam divergence angle were small as the screen grid thickness ratio varied from 0.062 to 0.247. The greatest normalized perveance-per-hole value was obtained with a value of $t_s/d_s = 0.123$. Ion recombination along the screen hole wall altering the local ion density and screen hole plasma sheath shape is believed to be the mechanism by which screen grid thickness variations slightly affect beamlet ion trajectories.

In summary, Figs. 5-8 show that ion beam divergence depends most strongly on normalized perveance per hole, grid separation ratio, and net-to-total accelerating voltage ratio changes. Also, the maximum normalized perveance per hole depends most strongly on the accelerator hole diameter ratio. Variations to the other geometrical grid parameters have a small effect on ion beam divergence. These same trends have been reported previously for 600 V total accelerating voltage operation,[18] indicating their general nature.

Figure 9 shows the effect of discharge voltage variations V_D on ion beam divergence for a total accelerating voltage V_T of 600 V. The grid geometry parameters remained at the values: $\ell_g/d_s = 0.494$, $d_a/d_s = 0.642$, $t_s/d_s = 0.185$, and $t_a/d_s = 0.370$. Increasing the discharge voltage, for a constant total accelerating voltage, shifts each beam divergence curve to lower normalized perveance-per-hole and ion beam divergence angle values. This effect is quite pronounced in Fig. 9 where a 3 deg average beam divergence angle decrease is observed for a discharge voltage increase from 32 to 50 V††. Higher total accelerating voltages of 1100 and 1500 V were investigated also over the same discharge voltage range. The angular spread caused by discharge voltage variations decreased with increasing total accelerating voltage. Figure 10 combines beam divergence data from from four different total ac-

††It should be noted that argon double ion production within the discharge chamber plasma has been shown to be small for discharge voltages up to 50 V.[19]

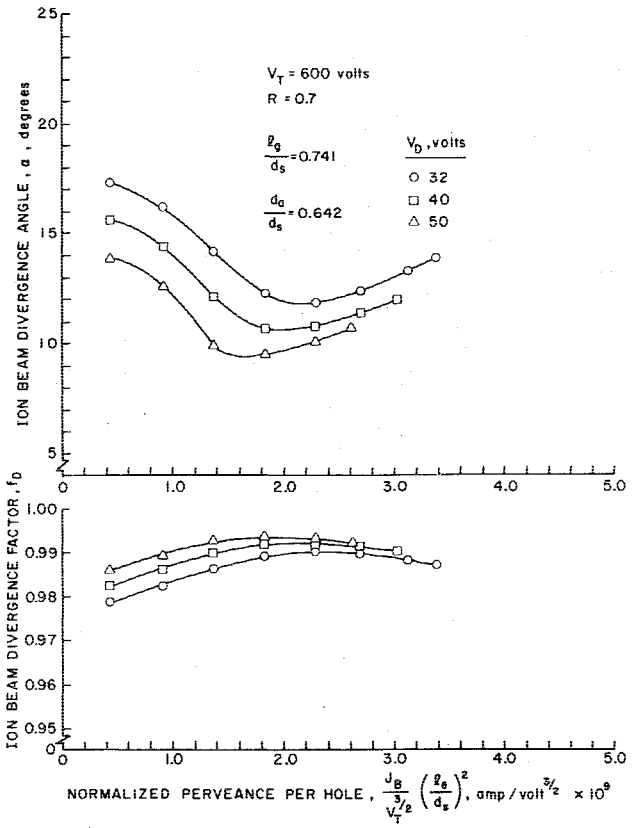

Fig. 9 Effect of discharge voltage V_D on ion beam divergence (total accelerating voltage $V_T = 600$ V).

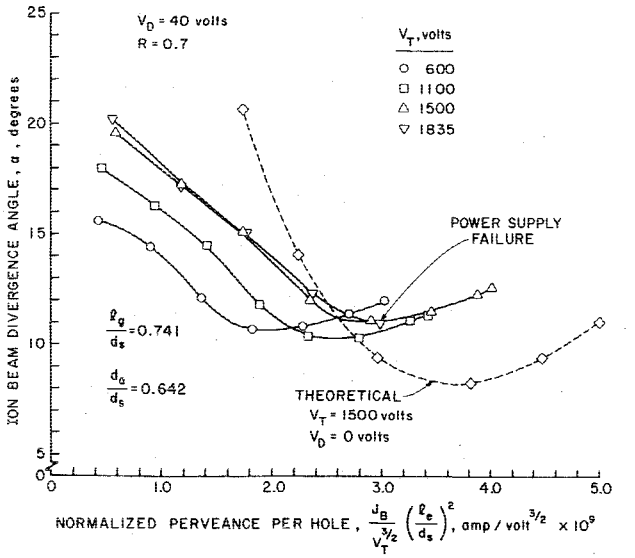

Fig. 10 Effect of total accelerating voltage V_T on ion beam divergence (discharge voltage $V_D = 40$ V).

celerating voltages using a 40 V discharge. Increasing the total accelerating voltage is shown to shift each beam divergence curve to higher normalized perveance-per-hole values. This effect decreases with increasing total accelerating voltage. The data contained in Figs. 9 and 10 show that neither total accelerating voltage nor discharge voltage alone adequately describe the beam divergence variations. From the observed opposite trends that increases in V_T and V_D produce, together with dimensional considerations, the ratio of these two parameters V_D/V_T is believed to be the most important quantity to describe the overall effect. Discharge and total accelerating voltage variations are believed to alter the screen hole sheath shape and position. However, the manner in which these changes occur to produce the results shown in Figs. 9 and 10 is still open to conjecture and is the object of further study. It can be said, though, that these changes have less effect on the beam divergence characteristics of a particular grid geometry as the discharge-to-total accelerating voltage ratio is decreased. Figure 10 shows also theoretical results obtained by Kaufman.[4] These theoretical results were based on a zero discharge voltage, and this is believed to be a major reason for their inability to model the experimental results adequately. Figure 10 indicates closer agreement between experiment and theory, as to location of the minimum beam divergence angle, as the experimental discharge-to-total accelerating voltage ratio approaches zero.

V. Correlated Results

In the previous section it was shown that ion beam divergence, from two-grid multiaperture accelerator systems, depends primarily on the normalized perveance per hole, grid separation ratio ℓ_g/d_s, net-to-total accelerating voltage ratio R, and discharge-to-total accelerating voltage ratio V_D/V_T. These four parameters have been used to correlate the ion beam divergence angle variation for all grid set geometries and accelerator system operating conditions examined during this study. Figure 11a shows the result of this correlation.

Here the simple Child's law normalized perveance-per-hole expression has been modified to include the effect of discharge-to-total accelerating voltage ratio variations. The ion beam divergence angle correlation is fairly good, with most of the data lying within a band $\pm 1\frac{1}{2}$ deg (actual degrees) of the indicated line of best fit. The parameter $NP/H_{\alpha_{min}}$ occuring in the beam divergence angle correlation refers to the normalized perveance per hole at the minimum beam divergence angle. It is plotted as a function of the discharge-to-total accelerating voltage ratio V_D/V_T and shown in Fig. 11b. It was necessary to introduce normalized perveance per hole as a parameter in the correlated beam divergence angle expression α_{corr} because of the decreased effect net-to-total accelerating voltage ratio variations have on the ion beam divergence angle at low normalized perveance-per-hole values (Figs. 5 and 6). Figures 11a and 11b allow ion beam divergence angles to be determined for a wide variety of grid geometry and accelerator system operating conditions. However, as mentioned previously in Sec. IV, there is an absolute beam current limit, related directly to the accelerator hole diameter ratio, for each grid set geometry. This limit is shown graphically in Fig. 11c. Figure 11c may be interpreted also as describing the beamlet diameter ratio d_b/d_s at the accelerator hole entrance as a function of the correlated normalized perveance per hole. This is because the beamlet diameter is approximately equal to the accelerator hole diameter at the maximum normalized perveance-per-hole (or beam current) condition. Figures 11a, 11b, and 11c should be used in the following way. First, the values of J_B, ℓ_e/d_s, V_D, V_T, and R must be known. The value of NP/H_{corr} is then calculated from the following expression:

$$\frac{NP}{H_{corr}} = \frac{J_B}{V_T^{3/2}}\left(\frac{\ell_e}{d_s}\right)^2\left(\frac{V_D}{V_T}\right)^{0.2} \tag{6}$$

This calculated value is used to obtain the value of α_{corr} from Fig. 11a. The value of $NP/H_{\alpha_{min}}$ is then found from Fig. 11b and used to calculate the actual beam divergence angle α, from the expression

$$\alpha_{corr} = \alpha\left(\frac{\ell_e}{d_s}\right)^{0.6}\left(\frac{V_D}{V_T}\right)^{0.2}\left(\frac{R}{0.9}\right)^{\frac{1.1NP/H}{NP/H_{\alpha_{min}}}} \tag{7}$$

Finally, Fig. 11c should be used to determine the minimum value of d_a to attain the desired beam current. To avoid excessive accelerator grid ion impingement this minimum d_a value should be increased by about 20%. If accelerator system

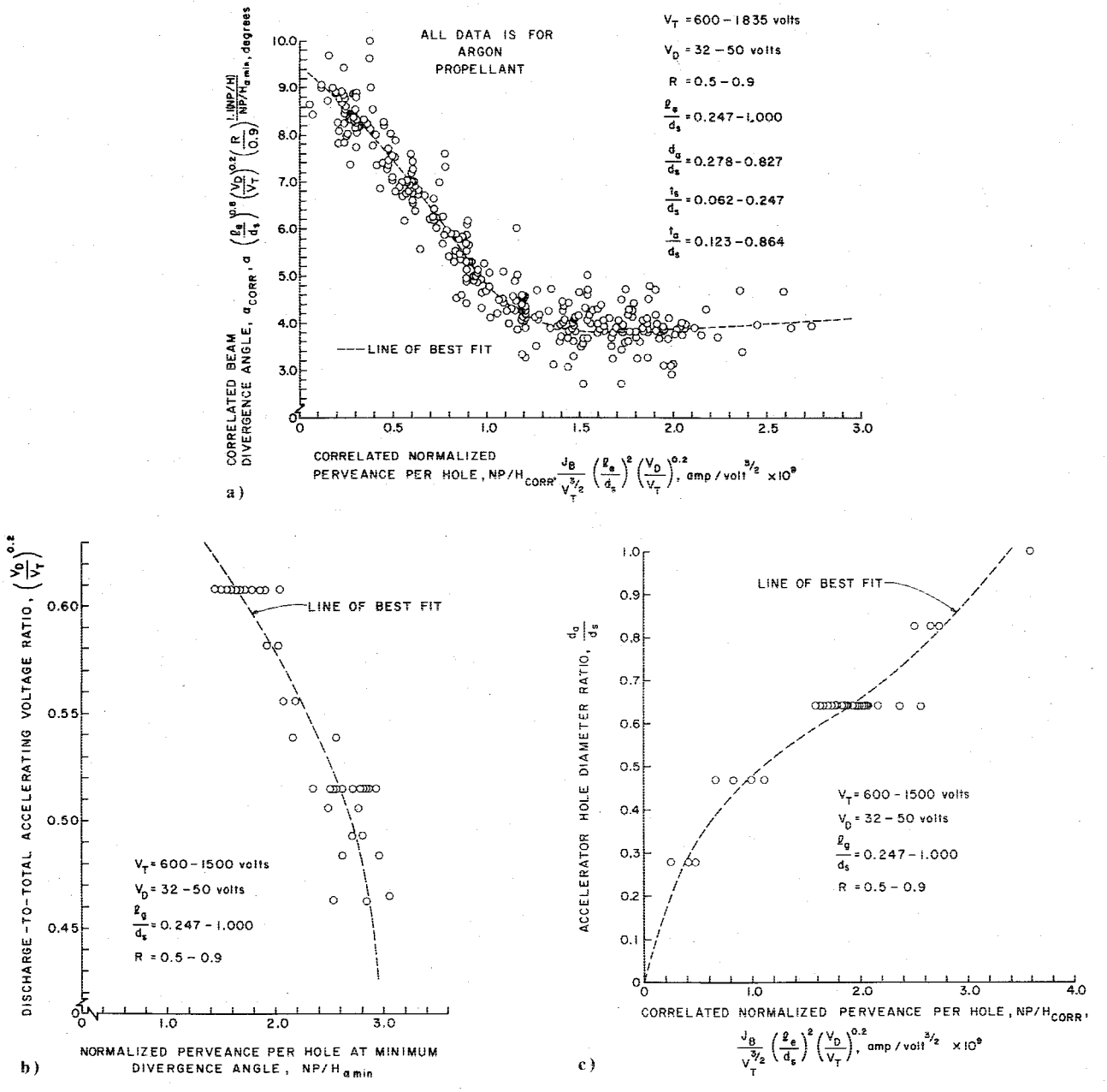

Fig. 11 a) Ion beam divergence angle correlation for all accelerator system operating conditions. b) Variation of the normalized perveance per hole at the minimum beam divergence angle $NP/H_{\alpha min}$ for discharge-to-total accelerating voltage ratio $(V_D/V_T)^{0.2}$ changes. c) Maximum normalized perveance per hole for accelerator hole diameter ratio d_a/d_s changes.

operation over a range of beam currents is proposed, Fig. 11c should be used to determine the value of d_a (by the method outlined earlier) necessary to attain the maximum beam current desired. The procedure outlined previously will then establish the range of divergence angles to be expected for the desired beam current operating range.

Figure 12 shows the minimum ion beam divergence angle that can be obtained as a function of grid separation ratio and net-to-total accelerating voltage ratio. A straight line was chosen as a conservative fit to the extrapolated regions which are considered to be good for a first approximation of the minimum beam divergence angle when operating at these extreme conditions. The data shown in Fig. 12 are most accurate for the discharge voltage and total accelerating voltage indicated. However, previous results (Figs. 9 and 10) have shown that varying V_D and V_T either side of 40 and 1100 V, respectively, produced a variation of $\pm 1\frac{1}{2}$ deg only in the minimum beam divergence angles given in Fig. 12. Hence, Fig. 12 may be used to obtain fairly representative minimum beam divergence angle trends for a wide range of discharge and total accelerating voltage ratios.

VI. Screen Hole Size and Propellant Variations

Figures 13 and 14 show the results of varying the two parameters held constant throughout this study: screen hole size and propellant gas. A constant grid aperture array size, similar nondimensionalized grid geometry parameters, and the same argon propellant mass flow rate were used for each screen hole size. Similar discharge chamber neutral number densities with the same grid system geometry were used for the different propellants. (An exception was neon which required twice the neutral number density of the other gases, a 46 V discharge, and a discharge chamber magnetic field reduction before a stable discharge plasma could be maintained.) Normalized perveance per hole for the different propellants shown in Fig. 14 was corrected for use with argon. This was done by multiplying each calculated normalized perveance-per-hole value [Eq. (3)] by the square root of the ratio of the

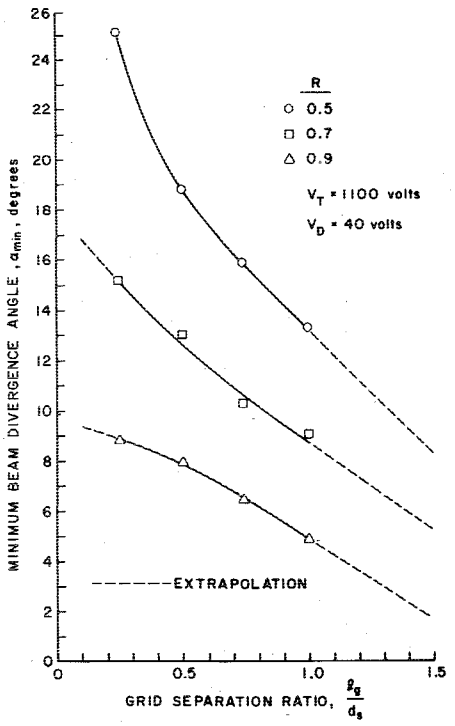

Fig. 12 Minimum ion beam divergence angle for grid separation ratio ℓ_g/d_s and net-to-total accelerating voltage ratio R changes.

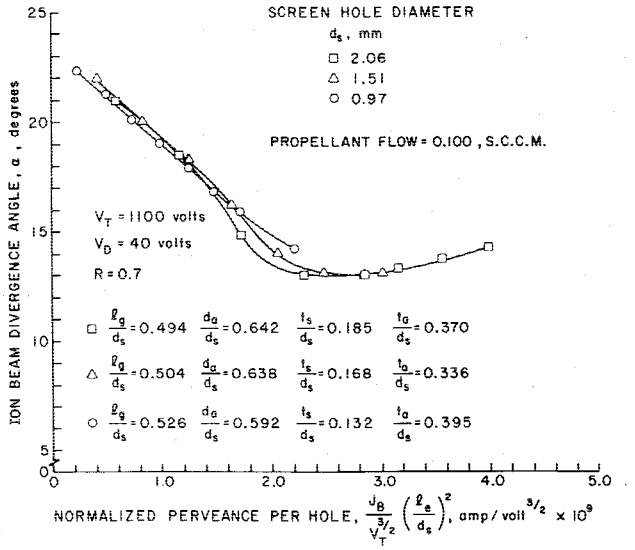

Fig. 13 Effect of screen hole diameter on ion beam divergence (similar nondimensionalized geometrical grid set parameters).

propellant atomic weight to the atomic weight of argon, (at. wt. prop./at. wt. argon)$^{1/2}$. The normalized perveance-per-hole reduction with decreasing screen hole size has been observed previously with two-grid electron-bombardment ion thrusters.[17] The present data verify those observations but do not shed new light on the cause of the effect.

Figures 13 and 14 show that screen hole size and propellant gas changes do not alter substantially the beam divergence variation found characteristic of a particular grid set geometry. Therefore, the data and correlation parameters presented in this report, while being most accurate for argon, are considered to hold generally for other propellants and screen hole sizes also. For instance, if knowledge of the ion beam divergence characteristics of a particular grid geometry operating with mercury rather than argon propellant is desired, then the following procedure should be used. From

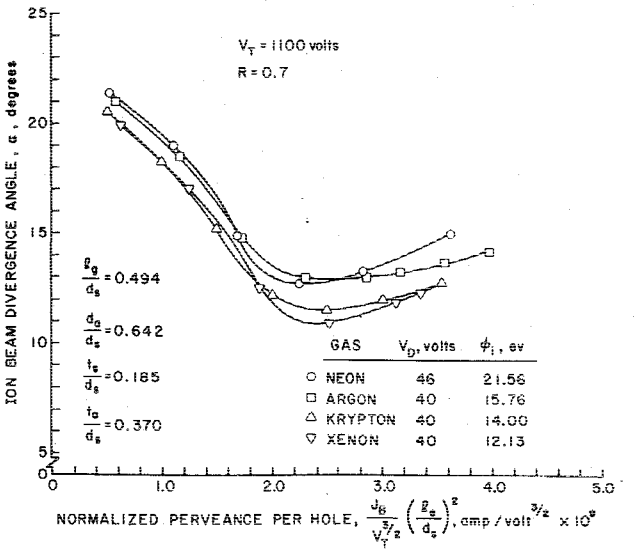

Fig. 14 Effect of propellant gas on ion beam divergence.

Eq. (3) the normalized perveance per hole is calculated for the grid set operating condition of interest (where M_i is now the atomic weight of mercury). This calculated normalized perveance-per-hole value is multiplied by the square root of the ratio of the atomic weight of mercury to the atomic weight of argon, (at. wt. mercury/at. wt. argon)$^{1/2}$ = 2.241. Now, having corrected the original value of normalized perveance per hole for mercury operation to a normalized perveance-per-hole value for use with argon, the data and correlation parameters presented in this report may be used.

VII. Conclusions

This work represents the first comprehensive experimental investigation of two-grid accelerator systems. A wide range of geometrical grid parameters and grid set operating conditions were investigated for their effect on ion beam divergence. Ion beam divergence was found to depend most strongly on normalized perveance per hole, grid separation ratio, net-to-total accelerating voltage ratio and discharge-to-total accelerating voltage ratio variations. The maximum normalized perveance per hole (or beam current) obtainable from a particular grid set, at a constant discharge-to-total accelerating voltage ratio, was found to depend most strongly on the accelerator hole diameter ratio. Variations of the other geometrical grid parameters have a small effect on ion beam divergence. The graphical results contained in this report provide guidelines for the design of ion accelerator systems. A general ion beam divergence angle correlation was developed to permit approximate beam divergence estimates, at parametric values other than those tested, of present and future grid set designs. All of the results contained in this report are considered of sufficient reliability to allow interpolation between specific experimental results and the use of limited range extrapolations. Although argon was the main test gas used in this study, the results are applicable to other propellants when the correction to normalized perveance per hole (as outlined in Sec. VI) has been made.

Acknowledgment

This work was supported by NASA under Grant NGR-06-002-112.

References

[1] Lockwood, D. L., Michelson, W., and Hamza, V., "Analytical Space-Charge Flow and Theoretical Electrostatic Rocket Engine Performance," *1st Electric Propulsion Conference*, Berkely, Calif., March 14-16, 1962.

[2]Hyman, J., Eckhardt, W. O., Knechtli, R. C., and Buckey, C. R., "Formation of Ion Beams from Plasma Sources: Part 1," *AIAA Journal*, Vol. 2, Oct. 1964, pp. 1739-1748.

[3]Lathem, W. C., "Ion Accelerator Designs for Kaufman Thrusters," *Journal of Spacecraft and Rockets*, Vol. 6, Nov. 1969, pp. 1237-1242.

[4]Kaufman, H. R., "Accelerator System Solutions for Broad-Beam Ion Sources," *AIAA Journal*, Vol. 15, July 1977, pp. 1025-1034.

[5]Aston, G., "Ion Optics Study," *15-cm Mercury Ion Thruster Research*, edited by P. J. Wilbur, NASA CR-134905, Dec. 1975, pp. 49-70.

[6]Bohm, D., "Minimum Ionic Kinetic Energy for a Stable Sheath," *The Characteristics of Electrical Discharges in Magnetic Fields*, edited by A. Guthrie, and R. K. Wakerling, McGraw-Hill, New York, 1949, pp. 77-86.

[7]Child, C. D., *Physical Review*, Vol. 32, 1911, pp. 492-511.

[8]Kaufman, H. R. and Reader, P. D., American Rocket Society, Paper No. 1374-60, 1960.

[9]Kaufman, H. R., NASA TN D-585, 1961.

[10]Aston, G., "The Ion-Optics of a Two-Grid Electron-Bombardment Thruster," NASA CR-135034, May 1976.

[11]Aston, G., "Ion Beam Divergence Characteristics of Two-Grid Accelerator Systems," *15-cm Mercury Ion Thruster Research*, edited by P. J. Wilbur, NASA CR-135317, Dec. 1977, pp. 154-160.

[12]Masek, T. D., Poeschel, R. L., Collet, C. R., and Schnelker, D. E., "Evolution and Status of the 30-cm Engineering Model Ion Thruster," AIAA Paper 76-1006, Key Biscayne, Fla., 1976.

[13]Hyman, J. Jr., Dulgeroff, C. R., Kami, S., and Williamson, W. S., "One-Millipound Mercury Ion Thruster," AIAA Paper 75-386, New Orleans, La., 1975.

[14]Robinson, R. S. and Kaufman, H. R., "Ion Thruster Technology Applied to a 30-cm Multipole Sputtering Ion Source," *AIAA Journal*, Vol. 15, May 1977, pp. 702-706.

[15]Kaufman, H. R., Reader, P. D., and Isaacson, G. C., "Ion Sources for Ion Machining Applications," *AIAA Journal*, Vol. 15, June 1977, pp. 843-847.

[16]Alterburg, W., Freisinger, J., Häuser, J., Seibt, N., and Loeb, H. W., "Beam Formation in RF-Ion Thrusters," AIAA Paper 75-426, New Orleans, La., 1975.

[17]Kaufman, H. R., "Technology of Electron-Bombardment Ion Thrusters," *Advances in Electronics and Electron Physics*, Vol. 36, Academic Press Inc., San Francisco, 1974, pp. 265-373.

[18]Aston, G. and Kaufman, H. R., "The Ion-Optics of a Two-Grid Electron-Bombardment Thruster," AIAA Paper 76-1029, Key Biscayne, Fla., 1976.

[19]Wilbur, P. J., "Argon-Xenon Discharge Chamber Model for the Production of Doubly Charged Ions," *Inert Gas Thrusters*, edited by H. R. Kaufman, NASA CR-135226, July 1977, pp. 46-64.